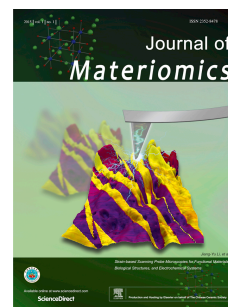


Journal Pre-proof

Flexible, tough and high-performing ionogels for supercapacitor application

Paulina Pietrzyk-Thel, Amrita Jain, Kamil Bochenek, Monika Michalska, Michał Basista, Tamas Szabo, Peter B. Nagy, Anna Wolska, Marcin Klepka



PII: S2352-8478(24)00027-3

DOI: <https://doi.org/10.1016/j.jmat.2024.01.008>

Reference: JMAT 833

To appear in: *Journal of Materiomics*

Received Date: 24 November 2023

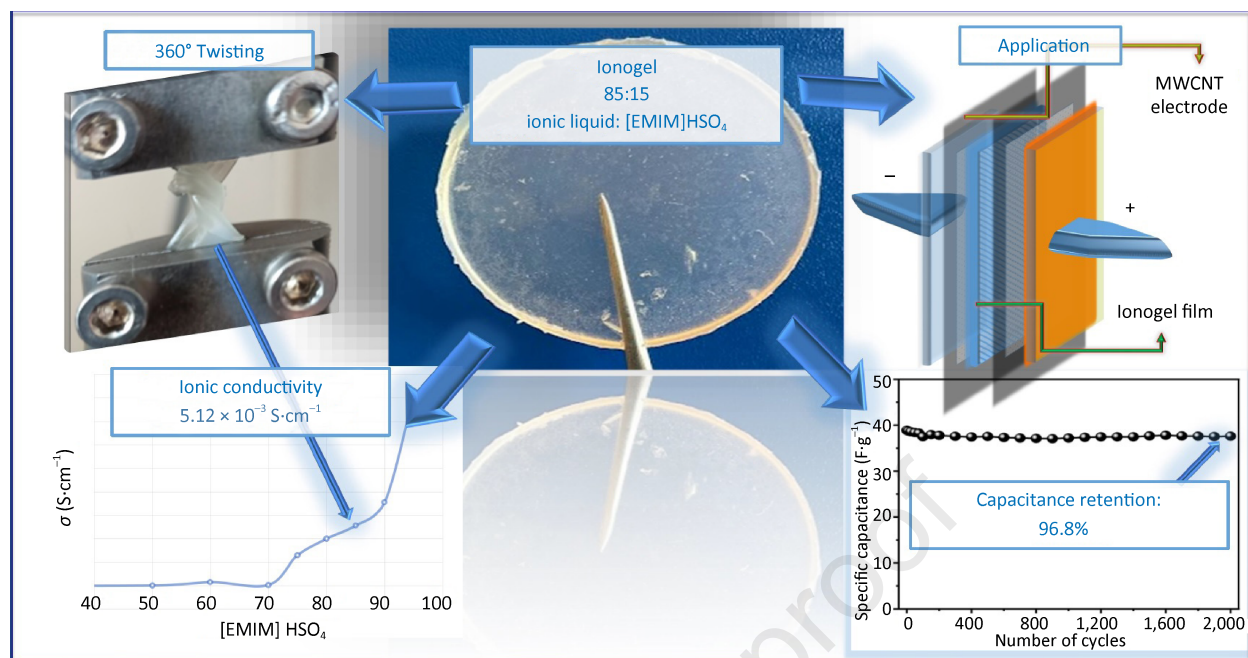
Revised Date: 12 January 2024

Accepted Date: 15 January 2024

Please cite this article as: Pietrzyk-Thel P, Jain A, Bochenek K, Michalska M, Basista Michał, Szabo T, Nagy PB, Wolska A, Klepka M, Flexible, tough and high-performing ionogels for supercapacitor application, *Journal of Materiomics* (2024), doi: <https://doi.org/10.1016/j.jmat.2024.01.008>.

This is a PDF file of an article that has undergone enhancements after acceptance, such as the addition of a cover page and metadata, and formatting for readability, but it is not yet the definitive version of record. This version will undergo additional copyediting, typesetting and review before it is published in its final form, but we are providing this version to give early visibility of the article. Please note that, during the production process, errors may be discovered which could affect the content, and all legal disclaimers that apply to the journal pertain.

© 2024 Published by Elsevier B.V. on behalf of The Chinese Ceramic Society.



Flexible, tough and high-performing ionogels for supercapacitor application

Paulina Pietrzyk-Thel^{1#}, Amrita Jain^{1#*}, Kamil Bochenek¹, Monika Michalska², Michał Basista¹, Tamas Szabo³, Peter B. Nagy³, Anna Wolska⁴, Marcin Klepka⁴

¹Institute of Fundamental Technological Research, Polish Academy of Sciences, Pawińskiego 5B, 02-106 Warsaw, Poland

²Department of Chemistry and Physico-Chemical Processes, Faculty of Materials Science and Technology, VSB-Technical University of Ostrava, 17. listopadu 2172/15, 708 00 Ostrava-Poruba, Czech Republic

³Department of Physical Chemistry and Materials Science, University of Szeged, Rerrich Béla Tér. 1, H-6720 Szeged, Hungary

⁴Institute of Physics, Polish Academy of Sciences, Al. Lotników 32/46, 02-668 Warsaw, Poland

*Corresponding author: ajain@ippt.pan.pl

#Equal contributors

Abstract

Ionogels are an attractive class of materials for smart and flexible electronics and are prepared from the combination of a polymer and ionic liquid which is entrapped in this matrix. Ionogels provide a continuous conductive phase with high thermal, mechanical, and chemical stability. However, because of the higher percentage of ionic liquids it is difficult to obtain an ionogel with high ionic conductivity and mechanical stability, which are very important from an application point of view. In this work, ionogel films with high flexibility, excellent ionic conductivity, and exceptional stability were prepared using polyvinyl alcohol as the host polymer matrix and 1-ethyl-3-methylimidazolium hydrogen sulfate as the ionic liquid using water as the solvent for energy storage application. The prepared ionogel films exhibited good mechanical stability along with sustaining strain of more than 100% at room temperature and low temperature, the ability to withstand twisting up to 360° and different bending conditions, and excellent ionic conductivity of 5.12×10^{-3} S/cm. The supercapacitor cell fabricated using the optimized ionogel film showed a capacitance of 39.9 F/g with an energy and power densities of 5.5 Wh/kg and 0.3 kW/kg, respectively confirming the suitability of ionogels for supercapacitor application.

Keywords: Ionic liquid; Gel polymer electrolyte; Ionic conductivity; 1-Ethyl-3-methylimidazolium hydrogen sulfate; Supercapacitors

Introduction

The urgent need to protect and save the natural resources and regulate the energy usage encouraged the research community to explore the sustainable materials and renewable energy storage system (EES). Supercapacitors are one of the representatives of EES systems that meet these needs, together with the fact that supercapacitors offer exciting features such as a fast charging-discharging rate, long cycling life, and high power density [1–3]. The primary challenge is to ensure the safety of any EES device. The organic liquid electrolytes which are considered as an origin of EES devices (especially traditional supercapacitors) are highly flammable, leaky, and volatile in nature. Polymer separators which are used to soak; these liquid electrolytes have poor thermal stability, leading to undesired accidents such as short circuits, overcharging, and overheating, these are known as thermal runaway. Thermal runaway occurs when the electrolyte decomposes or the gas is released, causing strong exothermic reactions that result in the explosion of the EES device. Therefore, the development of an electrolyte with safety as the top priority has become a major goal, leading to the safety of all EES device.

One of the possible solutions that the research community has focused on is the development of solid polymer electrolytes (SPEs), which have been relatively successful in overcoming the above challenges and drawbacks of liquid electrolytes. However, the problem with SPEs is a significantly high interfacial impedance and low ionic conductivity at room temperature. Furthermore, by combining the advantages of liquid electrolytes and SPEs, a gel polymer electrolyte (GPE) has been investigated as a promising electrolyte material for EES applications. Advantages of GPE include good electrical conductivity and acceptable mechanical stability. In GPEs, liquid electrolytes are entrapped in the polymer matrix without leakage. Here, the replacement of liquid electrolytes with ionic liquids (ILs) can significantly improve the safety of an EES device because the volatility of ILs is negligible compared to organic liquid electrolytes, and they have high electrochemical stability [4]. ILs are molten at room temperature and consist of cations and anions. The nature of the ions present in the ILs affects the chemical/electrochemical and physical properties [5] such as the electrochemical stability window, as well as the melting point or viscosity, which in turn affects the ionic conductivity of the overall system. ILs improve the performance of EES devices, ILs with imidazolium ions such as 1-butyl-3-methylimidazolium hexafluorophosphate ([BMIm]PF₆), 1-ethyl-3-methylimidazolium bis (trifluoromethylsulfonyl)imide ([EMIm]TFSI) [6,7], 1-ethyl-3-methylimidazolium hydrogen sulfate ([EMIM]HSO₄) have high ionic conductivity. Therefore, in addition to their hydrophilic nature, they are considered favorable candidates for EES applications[8,9]. Instead of using them as liquid electrolytes[10], the design of solid electrolytes with ILs, also called ionogels, is of great interest. The host network can be polymer-based, silica-based, or hybrid organic-inorganic based. Also, large organic molecules have been used for the preparation of electrolytes like hexamethylphosphoric triamide (HMPA) [11], 2, 7-dinitropyrene-4, 5, 9, 10-tetraone (DNPT) [12] and α , α' -dichloro-p-xylene [13] for energy storage applications.

Along with the above materials, choosing appropriate polymer also plays a major role as it decides the final results of the film. Various types of polymers have been used and reported as host polymers for gel electrolytes for use in EES applications. These polymers include poly(vinylidene fluoride-co-hexafluoropropylene) (PVdF-HFP), poly(vinyl alcohol) (PVA),

poly(methyl methacrylate) (PMMA), poly(ethylene oxide) (PEO), poly(acrylonitrile) (PAN) and copolymers of the above mentioned polymers [14–16]. Among all the polymers, PVA is one of the most studied and promising polymers because of several advantages, like easy availability, environmentally friendly, cost-effective, and most importantly, it has good compatibility with various salts and other components. Several research groups have used PVA to prepare different types of electrolyte materials, for example, Naveen *et al.*[17] prepared a biopolymer film using PVA with chitosan by casting method and magnesium chloride as salt. The maximum room temperature ionic conductivity of this film was $\sim 5.9 \times 10^{-5}$ S/cm. Similarly, Huang *et al.*[18] mixed epoxy resin with PVA to coat carbon nanofibers to prepare an electrolyte material. This approach resulted in an increase in conductivity to the order of $\sim 3.18 \times 10^{-2}$ S/m. However, Priya *et al.*[19] prepared a film using PVA as the polymer and mixed it with starch and a 2.0% solution of ceric ammonium nitrate to obtain an ionic conductivity of $\sim 1.53 \times 10^{-5}$ S/cm and the electrochemical stability window in the range of -2.0 V to $+2.0$ V. The prepared films were used for electrochemical double layer capacitors.

In the present work, the ionogel films with excellent electrochemical conductivity ($\sim 5.12 \times 10^{-3}$ S/cm) and superior mechanical properties were optimized and prepared by solution casting technique using PVA as the host polymer and 1-ethyl-3-methylimidazolium hydrogen sulfate as the ionic liquid, which is very compatible with PVA, resulting in the increased mobility of the polymer chain. The films were tested electrochemically and mechanically for energy storage application, specifically supercapacitors. For application testing, multiwalled carbon nanotubes (MWCNT) were used as the electrode material and a two-electrode cell was fabricated and characterized by electrochemical impedance spectroscopy (EIS), cyclic voltammetry (CV), and galvanostatic charge-discharge test (GCD) with cyclic testing. To the best of our knowledge, the ionogels with the proposed composition are used for the first time with MWCNT-based electrodes. It was also expected from the studies that the prepared ionogel has wide possibilities in flexible and smart EES devices.

Experimental section

Materials

Poly (vinyl alcohol) (PVA) with molecular weight, $M_w = 146,000$ - $186,000$, 87%–89% hydrolyzed, ionic liquid; 1-Ethyl-3-methylimidazolium hydrogen sulfate [EMIM]HSO₄ were purchased from Sigma Aldrich. Double-distilled water was obtained using the HydroLab purification system (Germany). Multiwalled carbon nanotubes (MWCNT $\geq 98\%$ carbon basis) were obtained from Sigma-Aldrich. The materials were used as received. Carbon cloth was purchased from AVCarb (USA).

Ionogel: preparation and characterization

The ionogel film was prepared using the standard solution casting technique. 0.3 g of PVA was dissolved in 30 mL of double-distilled water with a magnetic stirrer at 90 °C overnight and after dissolution it was gradually cooled down to room temperature. Meanwhile, 2.7 g of [EMIM]HSO₄ was homogeneously dissolved in 5 mL of double-distilled water in a separate beaker, for ~ 1 h at room temperature. The IL solution was then poured into the PVA solution

and stirred continuously for ~ 12 h. This solution was later poured into glass petri dishes and the common solvent (double-distilled water) was gradually allowed to evaporate slowly at room temperature. Free-standing and flexible ionogels were obtained after complete evaporation. Fig. 1 shows a schematic diagram of how ionogels were prepared. After this, the films were kept in a desiccator with desiccant to control the moisture content. Polymer films were obtained with different weight ratios of ionic liquid and [EMIM]HSO₄ polymer (95:5, 90:10, 85:15, 80:20, 75:25, 70:30, 60:40 and 50:50). The resulting ionogels were free-standing and mechanically stable films as shown in the schematic diagram (Fig. 1). The composition of optimized ionogel was used in the supercapacitor with MWCNT as the electrode material.

Fig. 1. Preparation scheme of the ionogel synthesis

The shear and oscillatory rheology measurements were carried out via a stress-controlled rheometer (MCR 302, Anton Paar) fitted with double gap, concentric cylinder geometry (CC27-SN12793). Controlled shear stress tests were conducted by varying the shear rate. Rheological studies were conducted at a constant temperature (25 °C) and atmospheric pressure. After loading, the samples were held for 5 min at the test temperature before measurements to allow stress relaxation and temperature equilibration. During the rotational tests, a range of shear rate from 1 to 1,000 s⁻¹ was applied, while shear stresses were recorded at different shear rate values. Data were collected using Anton Paar RheoCompass software. Morphological studies of the ionogels were performed by field emission scanning electron microscopy (FESEM) using SEM/FIB-Zeiss Crossbeam 350 and energy dispersive spectroscopy. To improve the conductivity of the surface, a thin layer of gold was deposited on the sample. EDS mapping and analysis were carried out using an Ametek EDAX, Octane Elite. Fourier transform infrared (FT-IR) study (Thermo Scientific Nicolet iS10 FTIR Spectrometer) was used to analyze the prepared films in the range of 500 to 4,000 cm⁻¹ with a resolution of 2 cm⁻¹ using the Attenuated Total Reflectance (ATR) mode with the Smart iTX attachment. A sample was placed on the diamond measuring window on the ATR attachment where the spectrum was collected. Each spectrum consisted of at least 64 scans lasting for ~ 1 s. Before each measurement, the background was collected to eliminate apparatus and environmental effects. Each sample spectrum is rationed. X-ray diffraction (XRD) analysis was performed by a Philips PW1830 diffractometer operating with an X-ray tube emitting Cu K α radiation, with 40 kV acceleration voltage at 30 mA current. The diffraction data were collected with a count time of 0.5 s per step and a sampling width of 0.04°. Cu plates were used as sample holders. PVA and the ionogel samples were cut into rectangular cuboid shapes and positioned onto the groove of the sample holder to align to the center of the goniometer circle. Samples were measured at approximately 28 °C and low humidity level (about 30%). Differential scanning calorimetry, (DSC–TG) was performed on TG/DSC SDT 650 simultaneous thermal analyzer, TA Instruments, to observe the possible phase transition due to the temperature change under the Ar atmosphere from room temperature to 400 °C at a heating rate of 5 °C/min. Thermogravimetric analysis (TGA) was performed using a Perkin-Elmer model TGA 8000 thermogravimeter (Shelton, USA) to obtain knowledge about the thermostability of the

optimized ionogel film. The measurement was carried out from 35 °C to 400 °C in a nitrogen atmosphere (AIR LIQUIDE POLSKA Sp. z o.o. - Kraków, Poland) with a temperature rate of 10 °C and a balance purge flow 40 mL/min. The mechanical properties of the prepared ionogels were examined using stress-strain curves obtained using the Kammrath-Weiss module with a highly sensitive 50N load cell and a maximum displacement rate equal to 20 μm/s. The *in-situ* tensile tests and ionic conductivity measurements were performed on Zwick ProLine Z050 universal testing machine in combination with SP-50e, BioLogic Instruments. Torsional strength was also investigated on Zwick Z050 by manually rotating the holders mounted on the machine. For both tests, 8 mm x 30 mm strips were cut from the manufactured films. XPS measurements were performed with a Scienta R4000 hemispherical analyzer (pass energy 200 eV) and monochromatic Al K α (1,486.7 eV) excitation (Scienta MX-650) working with a power of 150 W. The full width at half maximum (FWHM) of the 4f $_{7/2}$ Au line measured under the same experimental conditions was 0.64 eV. The sample was measured “as received”. The energy scale was calibrated, setting the C–C bond at 285 eV. The spectra were analyzed using the commercial CASA XPS software package (Casa Software Ltd., version 2.3.17) with the Shirley background. The Gaussian-Lorentzian functional - GL(30) was applied during the simulations.

The ionic conductivity of the ionogels was measured by electrochemical impedance spectroscopy technique (EIS) using a BioLogic VMP3 instrument in the frequency range of 1 Hz to 100 kHz with a signal range of 10 mV. To record this data, an electrochemical cell: stainless steel|ionogel|stainless steel was used. The ionic conductivity of the ionogels was calculated using the equation:

$$\sigma = \frac{l}{R_b A} \quad (1)$$

where, l is the thickness of the ionogel film, R_b is the bulk resistance of the cell, and A is the cross-sectional area of the stainless steel electrode.

The variation in ionic conductivity with temperature was measured using an *in-situ* experimental set-up. The potentiostat SP-50e, BioLogic instrument was connected with an atmospheric chamber (CTS climate temperature system, type C-20/350, CTS Germany, series number 107073), the temperature varied from 25 °C to 100 °C at a rate of 5 °C. Three readings were recorded at each temperature and the average was used for analysis. The optimized ionogel film was cut into 1 cm 2 and sandwiched between stainless steel electrodes and the ionic conductivity was measured. The ionic conductivity of the ionogel film was calculated using equation 1 at each temperature. From the temperature dependence data, the dielectric constant (ϵ^*) and modulus (M^*) were obtained and the equations used are given in the Supplementary Information (Equations S1–S4).

Fabrication of electrodes and supercapacitor cell

The commercial MWCNT material was used to prepare the electrodes for supercapacitor cells. To prepare the electrode materials, MWCNT and polyvinylidene fluoride (PVDF) as a binder were mixed using agate mortar in a ratio of 90%:10% (in mass) for ~30 min. Later, acetone was used as a common solvent to make a slurry of the mixture, which was finely

spread over the carbon cloth. The electrodes were left to dry for ~5–6 h at 40 °C which allowed the common solvent to evaporate. The average weight of the electroactive material was ~2.5 mg and the area of the electrodes was fixed to 1 cm². To fabricate the two-electrode supercapacitor cells, two symmetrical electrodes were placed on top of each other with the optimized ionogel film sandwiched in between. The configuration of the prepared cell was as follows:

Cell A: MWCNT|Ionogel (PVA:[EMIM]HSO₄)|MWCNT

The electrochemical performance of the prepared supercapacitor cell was evaluated using electrochemical impedance spectroscopy (EIS), cyclic voltammetry (CV), and galvanostatic charge-discharge (GCD) cycles with repeated cycling stability. The measurements were carried out using the BioLogic VMP3 instrument. The formulas used to calculate the capacitance values, energy, and power density of the prepared cell are provided in the Supplementary Information (equations S6-S10).

Results and Discussion

A well-mixed and homogeneous solution of PVA and [EMIM]HSO₄ was prepared using double-distilled water as the co-solvent, and after complete evaporation of the water, free-standing films were obtained. The composition of the ionogel was varied with respect to the percentage of the host polymer matrix, PVA (5%–50%, in mass) and the rest of the amount was ionic liquid. The as-prepared ionogels were named according to the percentage of the ionic liquid used (IL:X; X = 95%, 90%, 85%, 80%, 75%, 70%, 60% and 50%). All prepared films were mechanically stable (except 95:5) with no signs of liquid leakage. However, to achieve the best performing ionogel, thermal stability, ionic conductivity, and mechanical stability at room temperature were selected as the main parameters. The ionic conductivity of the 85:15 film was also tested at –20 °C.

Dynamic viscosity measurements

To obtain information on the rheological behavior of ionic liquid/water mixtures, the rheological curves were recorded using a rotational viscometer. Based on the trends shown in Fig. 2a, it can be concluded that for all systems in the investigated [EMIM]HSO₄/water volume ratio range, the viscosity curves are flat except for the first few points so that the mixtures can be considered as Newtonian fluids. However, the rheological properties depend on the chemical composition of the IL (chain length, type of anion/cation), and no shear thickening or shear thinning effect was observed as reported elsewhere[20]. It should be noted that the first few points deviate from the trend; this corresponds to the error of the method. It is more relevant at lower IL/water ratios since lower measured viscosity values have a higher relative error because the sensitivity of the method significantly decreases around the lower threshold of the measurement range. When the structural features are correlated with the data presented, it is suggested that no structure formation has developed due to the effect of shear forces in the investigated IL/water volume regime, which confirms the suitability of the ionic liquid for ionogel preparation.

To obtain the concentration dependence of the viscosity of [EMIM]HSO₄/water mixtures, the measured shear stress-shear rate values were fitted by the Bingham and also by the Casson models (discussed in the Supplementary Information). Both models gave very similar dynamic viscosity values, as shown in Fig. 2b. As stated in the literature, the viscosity of ionic liquid-water mixtures is affected by the chemical composition of the IL (*i.e.* hydrophilicity of the ionic groups, chain length *etc.*). Changes in viscosity ultimately depend on the separation distance of the IL chains and their interaction with each other[21]. The viscosity increases gradually with the IL content, but in the higher IL content regime it rises by one order of magnitude. This may be due to the IL-IL electrostatic interactions dominating in the bulk and the decrease in the separation of the ionic charges. As the water content decreases, the separation of the ion pairs abruptly decreases, leading to a sharp increase in viscosity[22]. Theoretically, it can also be directly related to the average number of hydrogen bonds per ionic group, which increases significantly with increasing IL content, as found in the literature[23]. Eventually, the viscosity reaches ca. 310–320 mPa s for the [EMIM]HSO₄/water mixture with 5% water content. We also associate this viscosity with that of the ionogels. The reason is that the nominal water content of the IL is about 5% as reported by the manufacturer, and we assumed that the PVA-containing ionogels, which are equilibrated with ambient humidity, have the same water content of about 5%. We also assumed that the water content of the ionogels is independent of the PVA content. This is rationalized by the assumption that the more hygroscopic component (*i.e.*, the ionic liquid) determines the adsorbed humidity level of a composite ionogel sample.

Fig.2. Flow curve of the [EMIM]HSO₄/water mixture (a) and semilogarithmic plot of the dynamic viscosities of [EMIM]HSO₄/water in different percentages of volume of I L at 25 °C (b)

Morphological and structural studies

The morphological studies were performed using SEM and are shown in Fig. 3a–3b. As can be seen from the SEM image, when the polymer content is relatively higher, the granular structures were observed in the films confirming the crystal phase in the films. However, the film consisting of 50% (in mass) of PVA shows not only grains, but also similar needle structures, which is typical for the structure of PVA and is consistent with the literature[24,25]. Furthermore, the needle structures disappear with increasing of [EMIM]HSO₄ content which confirms the amorphous phase of the prepared films. Fig. 3c–3d shows the EDX spectra of the prepared films and confirms the presence of elements used to prepare the films.

Fig. 3. SEM images of (a) 50:50, (b) 85:15, and EDX spectra of (c) 50:50, (d) 85:15 ionogel films (IL:PVA)

To understand the structure of the prepared ionogels in detail, various spectroscopic and thermal analyses were performed, as shown in Fig. 4a–4e.

Fig. 4: (a) FTIR full scale spectra, (b) FTIR expanded spectra, (c) XRD diffractogram, and (d) DSC of ionogels ([EMIM]HSO₄:PVA) at 50:50, 75:25, 85:15, 95:5 ratio; e) TGA curve of ionogel with 85:15 ratio

To confirm the chemical composition of the prepared ionogels and to understand the possible ion-solvent-polymer interactions, FT-IR spectroscopy was performed and is shown in Fig. 4a in the range from 4,000 cm⁻¹ to 500 cm⁻¹, while the extended spectrum from 1,600 cm⁻¹ to 400 cm⁻¹ is shown in Fig. 4b. The important peak assignments are presented in Table 1.

The broad band at 3,421 cm⁻¹ is due to the limited intermolecular stretching of the alcohol O–H group. This band decreases with an increasing amount of ionic liquid. The doublet of peaks (marked “**”) in Fig. 4a) at 3,158 cm⁻¹ and 3,110 cm⁻¹ originates from vibration of the imidazole ring. In the range of 3,000–2,800 cm⁻¹ the peaks originate from stretching of the alkyl group. However, at 1,456 cm⁻¹ asymmetric bending of the CH₂ vibration occurs, but at 1,340 cm⁻¹ symmetric bending was recorded. According to this, the peak at 1,635 cm⁻¹ can be attributed to C=C vibration, and the asymmetric N–O group vibration. In addition, the band at 1,575 cm⁻¹ comes from N–H group bending as well as C=N group vibration, or possibly from aromatic C=C bond vibrations. This band is remarkable at higher ionic liquid concentrations. At 85% ionic liquid concentration, the band at 1,390 cm⁻¹ begins to appear, which can be attributed to the stretching of the C–N group in aromatic compounds. The doublet of peaks (marked “*” in Fig. 4b) at 1,224 cm⁻¹ and 1,174 cm⁻¹ represents a symmetric and “free” triflate ion band of SO₃ vibrations[26]. The signal located at 1,097 cm⁻¹ is related to the stretching of C–O in the crystal sequence of PVA. However, the band at 1,045 cm⁻¹ increases with increasing IL concentration and represents the stretching C–C group. The band at 870 cm⁻¹ is related to C–H bending in the aromatic ring. Furthermore, the peak located at 590 cm⁻¹ can be attributed to asymmetric deformation of SO₃[27–29]. There is also evidence of a small amount of water in the samples, which gives rise to some IR-absorption at about 1,600 cm⁻¹ (bending vibration of H₂O). However, it is not possible to quantify the water content of the samples by IR spectroscopy.

Table 1 Assignment of important FTIR peaks of PVA and [EMIM]HSO₄.

Wavenumbers corresponding to functional groups (cm ⁻¹)	Assignment
3,421	O–H group vibration from PVA
3,158; 3,110	Vibration of imidazolium ring
3,000–2,800	Stretching of alkyl group

1,635	Asymmetric stretching of N–O group, C=C vibration
1,575	N–H bending, C=N vibration
1,456	Asymmetric bending CH ₂
1,390	C–N group vibration
1,340	Symmetric bending vibration CH ₂
1,224; 1,174	Asymmetric stretching vibration of SO ₃ and “free” triflate ion band of SO ₃
1,097	C–O stretching
1,045	C–C stretching
870	C–H bending
590	Symmetric stretching vibration of SO ₃

The structure of the [EMIM]HSO₄-PVA ionogels was characterized by X-ray diffraction. Fig. 4c compares the X-ray diffractograms of several ionogels with a high (> 50%) IL content with that of a pure polyvinyl alcohol sample. PVA is generally considered to be a semicrystalline neutral (uncharged) polymer. The pristine PVA used in this study also shows a crystalline order, as shown by its Bragg-reflection at $2\theta = 19.5^\circ$. This diffraction peak is moderately wide and intense. However, compared to a melt-crystallized, compression-molded PVA film studied by Ricciardi *et al.*[30], this sample does not have a very strong and sharp reflection, indicating a lower degree of crystallinity. On the other hand, the microcrystalline domains are characterized for both PVA samples by an X-ray diffraction maximum at $d = 4.55 \text{ \AA}$, referring to polymer chains in a trans-planar conformation, packed in a monoclinic unit cell[31]. In the ionic liquid-swollen PVA ionogels of different compositions, the Bragg peak of PVA appears at exactly the same diffraction angles. This indicates that during the solvation of the polymers with the ionic liquid, the crystalline regions do not undergo structural changes, except for a possible partial “dissolution” to an amorphous swollen state. However, a complete swelling and full dissolution of the total amount of the crystalline PVA do not occur even at the highest IL contents of >90%, as indicated by the small shoulder at $d = 4.55 \text{ \AA}$. For the latter, [EMIM]HSO₄⁻ rich samples, another Bragg reflection becomes dominant, centered at $2\theta = 22.8^\circ$. Since its intensity, relative to that of the PVA peak, gradually increases with the [EMIM]HSO₄ content, we assign this reflection to a periodic structure of 3.90 \AA repeat distances within the ionic liquid. We are not aware of any other studies in the literature that provide deeper insight into the interpretation of this d -spacing, but general considerations suggest that it simply originates from an internal, dynamic short-range ordering or beyond

(over the first few solvation shells)[32]. Finally, it should be noted that none of the samples exhibited any other X-ray reflections at high diffraction angles ($2\theta > 30^\circ$), indicating the absence of any crystalline impurities (such as precipitated salts or other contaminants) in the ionogels.

In addition, to understand the thermal stability of the films, differential scanning calorimetry (DSC) measurements of the ionogels were performed from room temperature to 400 °C. From the measurements, the glass transition temperature (T_g) and melting temperature (T_m) of the films were evaluated. The values are listed in Table 2.

Fig. 4d shows the heating curves of the ionogel films. As can be seen from the curve of 50:50, the T_g was found to be at 38 °C, which is the lowest compared to other films, and as the percentage of the ionic liquid is increased, the T_g gradually moves to higher values. For the composition 95:5, the T_g is 43 °C which can be attributed to the reinforcement of PVA and [EMIM]HSO₄ by crosslinking. However, for the 75:25 film, the T_g value decreases subtly to 34 °C, which can be caused by the dehydration of PVA in the structure[33]. Then, in the range T_g –144 °C, there is a loss of solvent (water) for all samples (marked with a yellow color). Furthermore, the third downward peak in the curves can be attributed to the melting temperature (T_m). The T_m value increases with an increase in the percentage of [EMIM]HSO₄ in the films. However, the 75:25 composition has the highest T_m (181 °C), which can be attributed to a substantial amount of non-associated [EMIM]HSO₄ in the film. Moreover, it was also noticed that around 268 °C, a peak was observed in 50:50 film which could be due to the melting of the PVA crystal domains[34]. The ionogel films above 300 °C tend to degrade due to the pyrolysis effect (marked with a purple color).

To prove the phase changes in ionogel film, TGA measurement was performed for an optimized composition of ionogel (85:15). Fig. 4e shows the loss of ionogel mass during the heat process (red curve) and the derivative (blue curve). The first phase change can be clearly seen in the range from 35 °C to 135 °C, which can be related to the evaporation of the water from the sample. The second region (135–280 °C) of the curve with decreasing slope can be attributed to the slowly decreasing water from the polymer matrix [35], and melting of PVA crystal domains. The mass of the film above 282 °C precipitously decreases, which is appropriate for the pyrolysis effect. The results of the TGA analysis (water loss and pyrolysis temperature) are in agreement with the DSC measurements.

From the DSC and TGA measurements (Fig. 4d–4e), it was observed that the ionogel film consisting of 85:15 ratio contains a successful cross-linking between the polymer (PVA in the present case) and the ionic liquid ([EMIM]HSO₄ in the present case) as indicated by the fact that no other phases were detected in this film, and the glass transition temperature was increased as compared to the other films. Therefore, the structural and thermal studies confirm that the 85:15 ionogel film is suitable for energy storage device applications.

Table 2. DSC results of PVA: [EMIM]HSO₄ ionogels

Content (PVA:EMIM HSO ₄ ⁻)	T_g (°C)	T_m (°C)	ΔH (J/g)
50:50	38	174	377.85

75:25	34	181	393.82
85:15	43	168	107.60
95:5	43	170	115.43

The XPS measurements were performed on the 85:15 ionogel film. The elemental composition was found to be approximately 50.8% of C, 28.1% of O, 12.1% of N and 9.0% of S atoms which is (within error) in agreement with the EDX results.

In the C 1s spectrum (Fig. 5a) three components were distinguished at 285, 286.2 eV, and 286.7 eV, which can be attributed to the C–C, C–N and C–O/C–S bonds, respectively[36,37]. The S 2p line (Fig. 5d) consists of the $2p^{3/2}$ and $2p^{1/2}$ components with an energy separation of 1.2 eV. The energy position at 180.0 eV corresponds to sulphide oxides C–SO_x[37,38]. Sulfur in other forms was not detected. In the O 1s line (Fig. 5b) two components can be found, C–O at 531.6 eV and SO_x at 532.9 eV which is consistent with the analysis of the C 1s and S 2p spectra. The N 1s spectrum (Fig. 5c) was deconvoluted into 2 peaks at the energy of 400.0 eV and 401.7 eV, which were assigned to the C–NH and C=NH groups, respectively[39].

Fig. 5. High-resolution XPS scans of: (a) C 1s, (b) O 1s, (c) N 1s, and (d) S 2p_{3/2} of the 85:15 ionogel film

Ionic conductivity and electrochemical studies

The electrochemical properties of the prepared ionogels were evaluated by measuring the ionic conductivity at room temperature (RT) and also by varying the temperature (from room temperature to 100 °C), the electrochemical potential/stability window, and finally studying the dielectric and modulus loss to understand the ion transport efficiency. The composition of 85:15 ([EMIM]HSO₄:PVA) was optimized to provide good mechanical stability and ionic conductivity for its application in energy storage devices. The room temperature ionic conductivity of the optimized film was found to be of the order of 5.12×10^{-3} S/cm. The conductivity of the pure PVA film was found to be of the order of $\sim 1.63 \times 10^{-12}$ S/cm [40]. This clearly confirms that the addition of an ionic liquid not only increases the conductivity but also enhances the flexibility of the film. The ionic conductivity of all prepared films (95:5, 90:10, 85:15, 80:20, 75:25, 70:30, 60:40, and 50:50) is shown in Fig. 6a. It is evident from the graph that the ionic conductivity of films with 90% and 95% (in mass) of ionic liquid is high due to the high content of ionic liquid present in the film. However, the films were not mechanically stable (as shown in Fig. S1 in the Supplementary Information), especially the film with 95% (in mass) of ionic liquid was too fragile. Since it was not even possible to obtain a sample for mechanical testing, the film with 85% (in mass) of the ionic liquid was chosen and considered as the optimized composition of the ionogel in the present work. For the optimized composition, the ionic conductivity at –20°C was also recorded and it was found to be of the order of $\sim 1.76 \times 10^{-3}$ S/cm, reflecting that the conductivity was not affected by

lowering the temperature. Moreover, to understand the temperature dependence of the conductivity behavior, the optimized film (85:15) was also studied in the temperature range from 25 °C to 100 °C and is shown in Fig. 6b. As can be seen from the Fig., the temperature dependence plot can be clearly divided into two linear regions, the first between 25–70°C, where the conductivity gradually increases due to the change in dielectric constant, and the second between 85–100°C, where the ionic conductivity values abruptly decrease due to the dielectric loss[41]. Furthermore, the polymer film obtained has both crystalline and amorphous phases. The temperature dependence plot of the optimized ionogel follows the Arrhenius model[42] using the equation:

$$\sigma_{dc}(T) = \sigma_0 \exp\left(-\frac{E_a}{k_B T}\right) \quad (2)$$

where: σ_0 is pre-exponential factor, k_B is Boltzmann constant (1.38×10^{-23} J/K), E_a is activation energy (J/K).

The Arrhenius model assumes that the movement of cations within the polymer does not originate from the polymer host side and that the increase in the conductivity is due to cation transport, where the ions seek out immediately vacant sites [43]. The correlation coefficient for the linear range 30–70 °C is 0.99208 and for 85–100 °C, R^2 is approximately 0.95318. The activation energy (E_a) can be estimated from the slope of the curves and is assumed to be 0.23 eV for the first region and 1.58 eV for the second region. The lower value of E_a is related to fast charge transport and dissociation of crystalline forms present in the polymer film. Similar kind of results are reported in the literature [43–46].

The electrochemical stability window (ESW) is the most important parameter for the polymer matrix in energy storage devices. The concept of ESW defines an interval between the cathodic and anodic potential limits that characterize the suitability of the electrolyte material in EES devices[47]. Fig. 6c shows the ESW, which was determined using linear sweep voltamperometry (LSV), where the potential step was 5.0 mV between the applied voltage from –4.0 V to +4.0 V with stainless steel as the working electrode and the counter electrode at room temperature. It can be clearly seen that the part of the curve from –2.40 V to +2.41 V is linear (total potential window ~4.81 V), with no obvious significant oxidation and reduction, confirming the electrochemical stability of the ionogel film in this range. After ~2.41 V, oxidation of the ionogel film was observed. This wide electrochemical stability window confirms that the potential of the prepared film is sufficient for electrochemical double layer capacitors (EDLC).

Fig. 6. (a) Ionic conductivity of prepared ionogels as a function of the percentage of ionic liquid (inset shows the original photo of ionogel 85:15); (b) Temperature dependence of ionic conductivity of optimized ionogel (85:15) from room temperature to 100 °C and also at –20 °C and (c) Electrochemical stability window of optimized ionogel film

The real (ϵ_r) part and imaginary (ϵ_i) part of the dielectric permittivity (ϵ^*) for the optimized ionogel system at different temperatures (RT to 100 °C) with respect to frequencies are shown in Fig. 7a–7b. The equations used to calculate the dielectric parameters are provided in

Supplementary Information (equation S1–S4). As can be seen from the Fig.7a the value corresponding to the real part of the dielectric permittivity decreases with the increase of the frequency, which could be due to the dispersive behavior at the lower frequencies. On the other hand, the higher values of ϵ_r at lower frequency values are attributed to the gathering of charges at the interface of sample and electrodes, which is known as space charge polarization. However, both the real and imaginary parts (Fig. 7a–7b) increase with increasing temperature. This behavior can be explained by the fact that with the increase in the charge carrier density, the increase in the dissociation of aggregates in the ions is possible. Furthermore, a weak or rather poor relaxation was observed in the real part of the constant, which could be due to the segmental type of motion of the polymer chain. However, as the temperature increases, the relaxation frequency shifts to the higher side of the frequency, showing that with an increase in temperature, the polymer segment relaxes much faster than at a lower temperature, resulting in an increase in the conductivity of the whole system[48].

At lower frequencies, the electrode interface polarization is so strong that it suppresses the other types of relaxation processes[49], and thus an urge arises to further interpret the dielectric behavior by using modulus spectroscopy which to some extent cancels out the electrode polarization. This technique is basically used to understand the electrical relaxation data, charge transport processes such as conductivity relaxation mechanism, ion dynamics *etc.* with respect to frequency at different temperatures. Fig.7c–7d shows the real (M_r) and imaginary (M_i) parts of the complex modulus spectra, the formulas used to calculate the real and imaginary parts of the complex modulus spectra are given in Supplementary Information (equation S5). As can be seen from Fig. 7c, the real part of the modulus spectra (M_r) shows the dispersion with the increase in the value of frequency which saturates with the increase of the frequency value. The small values of M_r in the lower frequency region allow the easy and facile motion of the ions, the similar kind of pattern was observed in Fig. 7d, where there are relaxation peaks in the imaginary part which are centered in the dispersion region of the real part of the modulus spectra. It was also observed that as the temperature increases, the charge carrier's motion becomes faster, which results in a decrease in the relaxation time, and consequently shifts the peaks to the higher side of the frequency. This type of mechanism clearly confirms that the relaxation is thermally activated and the jumping and hopping of the charge carriers occurs. This finding supports the suitability of ionogels for energy storage application[50]. This type of behavior was also confirmed by plotting the loss tangent δ curve shown in Fig. 7e which clearly demonstrates that the intensity of the peaks of $\tan \delta$ increases with the increase in conductivity at higher temperature, again confirming that the charge carriers of the ions are thermally activated via hopping mechanism[51].

Fig. 7. Frequency dependence of (a) real part (ϵ_r), (b) imaginary part (ϵ_i) of dielectric permittivity, (c) real part (M_r), (d) imaginary part (M_i) of modulus spectra at different temperatures for optimized ionogel system, and (e) Loss tangent spectra of optimized film

Mechanical properties

As mentioned in the previous sections, the ionogel films were prepared by combining different ratios of the host polymer (in this case PVA) and the ionic liquid (EMIM-HSO₄). All of the prepared films were self-supporting, free-standing, and flexible in nature, which was visually confirmed. The aim of this work was to select a film with balanced electrochemical and mechanical properties. Ionogels with ratios of 85:15, 90:10, and 95:5 ratios exhibited excellent ionic conductivity at room temperature, which was supported by the electrochemical results. However, the ionogel with 95% (in mass) ionic liquid was mechanically unstable, making it impossible to carry out the mechanical test, which was apparently caused by the high concentration of ionic liquid. In view of the above, it was decided to limit the mechanical tests to only two ionic liquid compositions, namely 85:15 and 90:10. This decision was justified for two reasons: the lower ionic liquid content promotes mechanical strength, but the electrochemical properties quickly become less interesting for applications. Both films were particularly sensitive during handling and mounting into devices as a result of their low relative strength. However, it was possible to perform repeatable tests on both materials close to 100% of the total strain. Fig. 8a shows the stress-strain curves of the investigated specimens. It is clear that the mechanical properties decrease rapidly as the ionic liquid content increases. The difference in maximum strength exceeds 400%, indicating that the 85:15 composition has significantly better application properties. Furthermore, after 100% total elongation during loading, the plastic deformation of 85:15 was 35%, and that of 90:10 was 55%. Fig. 8b shows the 85:15 ionogel film during the tensile test on the Kammrath-Weiss module. The mechanical tests clearly demonstrate higher mechanical strength of the selected 85:15 composition.

Fig. 8. (a) Stress-strain curves for PVA:ionic liquid ionogel films with a ratio of 85:15, 90:10 and (b) Kammrath-Weiss tensile-compression module with the 85:15 film specimen mounted

Fig. 9. Images of ionic liquid films during strain level of 50% for (a) 85:15 and (b) 90:10; Torsional strength of the material performed by rotation of holders around the axis on Zwick Z050 UTM; (c) 85:15 film after 360° rotation (maximum angle reach approx. 375°); (d) 90:10 after 45° rotation, where maximum angle has barely surpassed 50°.

Due to the limited displacement rate of the KW module, further tests were performed on the Zwick Z050 Universal testing machine. Here, the films were stretched up to 50 and 100% of the initial length, and the ionic conductivity was measured after stretching. Naturally, a new specimen was used for each level of deformation. Fig. 9a shows 85:15 specimens at 50% strain. The material is opaque, but no defects or voids are visible to the naked eye. The 90:10 film at 50% of strain (Fig. 9b) is more transparent, but some defects are visible, and changes in the structure of material can also be observed during deformation.

Torsional tests of the materials around the axis also showed a higher strength of the 85:15 composition. The 90:10 film was damaged after more than 45° of rotation (Fig. 9d). For the 85:15, it was possible to rotate the specimen more than 360° (Fig. 9c).

Supercapacitor performance: application testing

Finally, the optimized ionogel was incorporated with a MWCNT electrode in a two-electrode setup as a complete cell to evaluate its performance as a supercapacitor. Fig. 10a–10d shows the performance characteristics of Cell A using different techniques such as EIS, CV, GCD and cyclic stability. The EIS as shown in Fig. 10a was performed in the frequency range from 100 mHz to 200 kHz. At higher frequencies, a small semicircular spur (extended version shown in the inset) was observed at the intercept on the X-axis (real part of the complex impedance, Z') showing the bulk and interfacial properties of the capacitor cell. In this semi-circular spur, two intercepts were observed. The first intercept represents the bulk resistance called as R_b (also marked in the inset), while the second intercept is called the charge transfer resistance R_{ct} (as marked in the inset). These resistances exist at the electrode/electrolyte interface. As can be seen from Fig. 10a, the semicircular spur is also followed by a steep rising pattern (almost $\sim 90^\circ$) which is parallel to the Y-axis (impedance part). This confirms the perfect supercapacitive characteristics of the ionogel-MWCNT cell and the suitability of the prepared ionogel for energy storage application. In the present case, the values of total resistance R , R_b and R_{ct} were found to be of the order of ~ 105.8 , $12.3 \Omega \cdot \text{cm}^2$ and $45.9 \Omega \cdot \text{cm}^2$, respectively. The capacitance values from the EIS technique were calculated using equation S6 in the Supplementary Information and were found to be of the order of $\sim 38.1 \text{ F/g}$. The high value of capacitance and low values of resistance clearly indicate the proper double layer formation and the easy and flawless movement of EMIM^+ and HSO_4^- ions through the pores of MWCNT electrodes.

Capacitive performance was further evaluated by CV measurements at different scan rates: 5, 10, 20, 50 mV/s and 100 mV/s and is shown in Fig. 10b. As can be seen from the Fig., the CV curves of cell A show a symmetrical and rectangular shape confirming the lower charge transfer resistance, and almost ideal capacitance behavior, which could be due to the higher ionic conductivity. In addition, no redox peaks were observed in the CV curves of cell A, which ensures that the cell has typical double layer electrochemical characteristics. Although a slight deviation was observed at higher scan rates, the overall CV studies confirmed the good compatibility of the interface between electrode and electrolyte. The capacitance value at a scan rate of 5 mV s^{-1} was calculated using Equation S7 in Supplementary Information and is found to be of the order of $\sim 39.9 \text{ F/g}$. Fig. S2 in Supplementary Information shows the variation of the specific capacitance with respect to the given scan rates. As can be seen in the Fig., the specific capacitance decreases with increasing scan rates, indicating the easy switching of electrolyte ions within the ions of the electrode material (MWCNT in this case).

The galvanostatic charge-discharge (GCD) measurement was also conducted at a current density of 1.2 A/g to confirm the performance characteristics of Cell A. The GCD curve shown in Fig. 10c is almost linear, which is attributed to the double layer capacitor with a minimal internal resistance (IR) drop of $\sim 31.6 \Omega \cdot \text{cm}^2$. This clearly demonstrates the low impedance of the device and the excellent contact between the electrode and the electrolyte. Similar

observations were also made from the EIS and CV measurements. The specific capacitance values, energy density, and power density values from the GCD measurement were evaluated using equations S7–S9 in the Supplementary Information, and were found to be of the order of ~ 39.4 F/g, 5.5 Wh/kg and 0.3 kW/kg, respectively. These results are in good agreement with the EIS and CV studies.

Fig. 10. (a) EIS plot of cell A at a frequency of 10 mHz; (b) CV curves of cell A at different scan rates; (c) GCD curve of cell A at a current density of ~ 1.2 A/g, and (d) variation of specific capacitance of cell A with respect to cycle numbers (the inset shows some GCD cycles during cyclic test measurements.)

Finally, cell A was subjected to prolonged cyclic testing using the GCD technique at a constant current density of ~ 0.2 A/g and a voltage range of 0 V to 1.0 V. Fig. 10d shows the variation of the discharge capacitance with respect to the number of cycles. As can be seen, there is a slight loss of capacitance values in the first few cycles, which could be caused by the slow kinetics at the electrode-electrolyte interface. Due to irreversible electrochemical reactions, the capacitance values remain constant throughout the cycles, and after $\sim 2,000$ cycles, 96.8% of the capacitance was retained, demonstrating the durability and excellent performance of the electrolyte material. The inset of Fig. 10d shows the first few GCD cycles during the cyclic test measurement. Fig. S3a–3b in the Supplementary Information shows the comparison of the EIS (at a frequency of 10 mHz) and the CV curves (at a scan rate of 10 mV/s) of cell A before and after the cycling test. As can be seen from the Fig.s, there is almost no change in the performance of the cell. This can be interpreted as evidence of the stability of the supercapacitor cell and the suitability of the prepared ionogel for energy storage applications. Table 3 shows a comparison of the literature results regarding the properties of ionic liquid based electrolytes used for different energy storage applications with the results obtained in this work.

Table 3. Comparison of electrolytes films obtained by using different polymer matrices and ionic liquid

No	Polymer / Ionic liquid/ substrate	Solvent/ Electrode material	Conductivity (S/cm)/ Electrochemical stability window (V)	Specific capacitance	Energy density	Power density	Cycling test	Application	Ref.
1	PVA/ Cassava starch	Cerium ammonium nitrate (2%)/ AC	1.53×10^{-5} / 4.00	29.45 F/g	1.60 Wh/ kg	0.099 kW/ kg	1,000	Super capacitor	[19]
2	EA + PETEA/ EMIC	Graphite	1.46×10^{-3} / 3.00	90.00 mA·h/g	100.00 mA/g		1,000	Aluminium battery	[52]
3	PVDF-HFP/ [EMIM][BF ₄]	[EMIM][BF ₄]/ AC	6.90×10^{-3} / 3.91	161.80 F/g	89.89 Wh/ kg	8.000 kW/ kg	10,000	EDLC	[53]
4	Poly(1-[2-(2-(2-(Methacryloyloxy)ethoxy)ethoxy)ethyl]-3-methylimidazolium bis(trifluoromethylsulfonyl)imide)-copoly(poly(ethylene glycol) methyl ether methacrylate) +	DMAc/ LiFePO ₄	1.76×10^{-3} / 4.26	143.00 mA·h/g			120	Lithium battery	[54]

	PVDF/ [BMIM]TFSI								
5	PVA/ EMICI	TMSI/ AC	$1.54 \times 10^{-2}/$ 2.90	613.00 F/g	69.00 Wh/ kg	0.305 kW/ kg	5,000	Super capaci tor	[55]
6	PVdF-co-HFP/ [EMIM][NTf ₂]	Acetone/ AC	$2.70 \times 10^{-3}/$ 3.50	130.00 F/g	28.20 Wh/ kg	0.391 kW/ kg	5,000	Super capaci tor	[56]
7	PVA/ [EMIM] [EtSO ₄]	Ammonium acetate/ LIG	$10.80 \times 10^{-3}/$ 2.00	15.10 mF·cm ⁻²	1.54 μ W·h/c m ²	0.920 mW/cm ²	5,000	Super capaci tor	[57]
8	PMM + PLA/ BmimCl	TEGDME/ LiTFSI	$1.63 \times 10^{-3}/$ 3.40					Lithiu m-ion batter ies	[58]
9	PVA/ EMIM-TCM	DMSO/ AC	$3.85 \times 10^{-4}/$ 4.00	32.40 F/g				EDLC	[59]
10	PVDF-HFP/ EMIMTFSI	TEOS + formic acid/ LFP + Li _{1,17} Ni _{0,27} Co _{0,05} Mn _{0,52} O ₂	$5.30 \times 10^{-4}/$ 4.90	194.30 mA·h/g			400	Solid lithiu m metal batter ies	[60]

11	PVA/ [EMIM] HSO ₄ ⁻	Water/ MWCNT	5.12 x10 ⁻³ / 4.81	39.40 F/g	5.50 Wh/ kg	0.300 kW/ kg	2,000	Super capaci tor	This work
----	--	-----------------	----------------------------------	--------------	----------------	-----------------	-------	------------------------	--------------

Journal Pre-proof

Conclusions

In this paper, a successful preparation of an ionogel using PVA as a polymer and [EMIM]HSO₄ as an ionic liquid for the supercapacitor application was discussed. The structural and morphological results confirmed that the ionic liquid was well entrapped in the host matrix. The ionic conductivity of the optimized ionogel was found to be of the order of $\sim 5.12 \times 10^{-3}$ S/cm, and due to the strong solvation of EMIM⁺ and HSO₄⁻ ions, the electrochemical potential window of the ionogels was significantly wide (~ 4.8 V). Further dielectric and modulus analysis showed that the framework of the host polymer of the ionogel helped in increasing the dielectric constant. This, in turn, helped to increase the energy storage and minimize the dielectric loss, which means that the energy loss due to the dissociation of ion pairs and the presence of segmental motion for the transport of ions is less. The ionogel films were also mechanically stable and easily twisted up to 360° with 100% total elongation under loading. The plastic deformation of the 85:15 film was $\sim 35\%$, which confirms that the prepared films are also well suited for flexible devices. The applicability of the ionogel in supercapacitor application was tested using MWCNT as electrode materials. The fabricated cell provided a capacitance of ~ 39.4 F/g with an energy density of 5.5 Wh/kg and a power density of 0.3 kW/kg. All results confirm that the prepared ionogels have potential for use in EES devices.

Author contributions

Paulina Pietrzyk-Thel: Investigation, Formal Analysis, Writing-original draft, Writing-Review and Editing, Visualization. **Amrita Jain:** Conceptualization, Investigation, Formal Analysis, Validation, Visualization, Writing-original draft, Writing-Review and Editing, Supervision, Funding Acquisition, **Monika Michalska:** Investigation, Visualization, Writing-original draft, Writing-Review and Editing, Funding acquisition **Kamil Bochenek:** Investigation, Writing-original draft. **Michał Basista:** Formal Analysis, Supervision, Writing-Review and Editing. **Anna Wolska:** Formal Analysis, Writing-Review and Editing. **Marcin Klepka:** Formal Analysis, Writing-Review and Editing. **Tamas Szabo:** Investigation, Formal Analysis, Writing-original draft, Writing-Review and Editing, Funding Acquisition. **Peter B. Nagy:** Investigation, Writing-original draft.

Declaration of competing interest

The authors declare that they have no known competing financial interests or personal relationships that could have appeared to influence the work reported in this paper.

Data availability

Data will be made available on request.

Acknowledgements

This work was financially supported by the National Centre for Research and Development (NCBR, Poland); Project number: V4-Japan/2/17/AtomDeC/2022 and the Ministry of Education, Youth and Sports, Czech Republic (contract no. 8F21007) and the NKFIH (project No. 2019-2.1.7-ERA-NET-2021-00029) under the Visegrad Group-Japan 2021 Joint Call on Advanced Materials in cooperation with the International Visegrad Fund. Authors would like

to thank Dr. Silvie Vallova (VSB-TUO) for thermal analysis results, Dr. K. M. Górecki (VSB-TUO) for FTIR measurements, and the Large Research Infrastructure ENREGAT (project No. LM2023056) supported by the Ministry of Education, Youth and Sports of the Czech Republic. Authors would like to acknowledge Prof. Michael Giersig and Dr Magdalena Osial, IPPT PAN (Poland) for TGA measurement.

References

- [1] Kim D, Kannan PK, Chung C. High-Performance Flexible Supercapacitors Based on Ionogel Electrolyte with an Enhanced Ionic Conductivity. *ChemistrySelect* 2018;3:2190–5.
- [2] Vannathan AA, Kella T, Shee D, Mal SS. High-performance electrochemical supercapacitors based on polyoxometalate integrated into polyaniline and activated carbon nanohybrid. *Ionics (Kiel)* 2023;29:4227–41.
- [3] Zhou H, Su Y, Zhang J, Li H, Zhou L, Huang H. A novel embedded all-solid-state composite structural supercapacitor based on activated carbon fiber electrode and carbon fiber reinforced polymer matrix. *Chemical Engineering Journal* 2023;454:140222.
- [4] Ruan Q, Yao M, Yuan D, Dong H, Liu J, Yuan X, et al. Ionic liquid crystal electrolytes: Fundamental, applications and prospects. *Nano Energy* 2023;106:108087.
- [5] Armand M, Endres F, MacFarlane DR, Ohno H, Scrosati B. Ionic-liquid materials for the electrochemical challenges of the future. *Nat Mater* 2009;8:621–9.
- [6] Yao M, Ruan Q, Pan S, Zhang H, Zhang S. An Ultrathin Asymmetric Solid Polymer Electrolyte with Intensified Ion Transport Regulated by Biomimetic Channels Enabling Wide-Temperature High-Voltage Lithium-Metal Battery. *Adv Energy Mater* 2023;13.
- [7] Ruan Q, Yao M, Luo S, Zhang W, Bae C-J, Wei Z, et al. A gradient “Ceramic-in-Ionogel” electrolyte with tidal ion flow for ultra-stable lithium metal batteries. *Nano Energy* 2023;113:108571.
- [8] Ma X, Yu J, Hu Y, Texter J, Yan F. Ionic liquid/poly(ionic liquid)-based electrolytes for lithium batteries. *Industrial Chemistry & Materials* 2023;1:39–59.
- [9] Han YK, Cheon JY, Kim T, Lee SB, Kim Y Do, Jung BM. A chemically bonded supercapacitor using a highly stretchable and adhesive gel polymer electrolyte based on an ionic liquid and epoxy-triblock diamine network. *RSC Adv* 2020;10:18945–52.
- [10] Catarineu NR, Lin D, Zhu C, Oyarzun DI, Li Y. High-performance aqueous zinc-ion hybrid capacitors based on 3D printed metal-organic framework cathodes. *Chemical Engineering Journal* 2023;465:142544.
- [11] Wang D, Lv D, Peng H, Wang C, Liu H, Yang J, et al. Solvation Modulation Enhances Anion-Derived Solid Electrolyte Interphase for Deep Cycling of Aqueous Zinc Metal Batteries. *Angewandte Chemie International Edition* 2023;62.
- [12] Song Z, Miao L, Lv Y, Gan L, Liu M. NH_4^+ Charge Carrier Coordinated H-Bonded Organic Small Molecule for Fast and Superstable Rechargeable Zinc Batteries. *Angewandte Chemie* 2023;135.

- [13] Zhang Y, Song Z, Miao L, Lv Y, Gan L, Liu M. All-Round Enhancement in Zn-Ion Storage Enabled by Solvent-Guided Lewis Acid–Base Self-Assembly of Heterodiatomic Carbon Nanotubes. *ACS Appl Mater Interfaces* 2023;15:35380–90.
- [14] Seok Jang H, Justin Raj C, Lee W-G, Chul Kim B, Hyun Yu K. Enhanced supercapacitive performances of functionalized activated carbon in novel gel polymer electrolytes with ionic liquid redox-mediated poly(vinyl alcohol)/phosphoric acid. *RSC Adv* 2016;6:75376–83.
- [15] Tseng Y-H, Lin Y-H, Subramani R, Su Y-H, Lee Y-L, Jan J-S, et al. On-site-coagulation gel polymer electrolytes with a high dielectric constant for lithium-ion batteries. *J Power Sources* 2020;480:228802.
- [16] Wu N, Cao Q, Wang X, Li X, Deng H. A novel high-performance gel polymer electrolyte membrane basing on electrospinning technique for lithium rechargeable batteries. *J Power Sources* 2011;196:8638–43.
- [17] Naveen C, Muthuvinayagam M. Studies on electrical properties of Chitosan-PVA based biopolymer electrolytes for electrochemical devices. *Journal of Polymer Research* 2023;30:353.
- [18] Huang F, Singer G, Zhou Y, Sha Z, Chen J, Han Z, et al. Creating ionic pathways in solid-state polymer electrolyte by using PVA-coated carbon nanofibers. *Compos Sci Technol* 2021;207:108710.
- [19] Nithya Priya C, Muthuvinayagam M, Vahini M. Environmental friendly solid blend polymer electrolytes based on PVA:starch:ceric ammonium nitrate for electric double layer capacitor (EDLC) applications. *J Mater Sci* 2023;58:773–86.
- [20] Takada A, Imaichi K, Kagawa T, Takahashi Y. Abnormal Viscosity Increment Observed for an Ionic Liquid by Dissolving Lithium Chloride. *J Phys Chem B* 2008;112:9660–2.
- [21] De Sarkar S, Mitra S, Ghosh SK. Relating the physical properties of aqueous solutions of ionic liquids with their chemical structures. *The European Physical Journal E* 2020;43:55.
- [22] Singh AP, Gardas RL, Senapati S. Divergent trend in density versus viscosity of ionic liquid/water mixtures: a molecular view from guanidinium ionic liquids. *Physical Chemistry Chemical Physics* 2015;17:25037–48.
- [23] Verma A, Stoppelman JP, McDaniel JG. Tuning Water Networks via Ionic Liquid/Water Mixtures. *Int J Mol Sci* 2020;21:403.
- [24] Aydemir D, Gündüz G, Aşık N, Wang A. The Effects of Poly(vinyl acetate) Filled with Nanoclay and Cellulose Nanofibrils on Adhesion Strength of Poplar and Scots Pine Wood. *Drvna Industrija* 2016;67:17–24.
- [25] Nagy ZsK, Nyul K, Wagner I, Molnar K, Marosi Gy. Electrospun water soluble polymer mat for ultrafast release of Donepezil HCl. *Express Polym Lett* 2010;4:763–72.
- [26] Parveen S, Hashmi SA. Flexible gel polymer electrolyte comprising high flash point solvent adiponitrile with ethylene carbonate as co-solvent for sodium-ion batteries. *J Energy Storage* 2023;67:107519.
- [27] Srinivasa Rao V, Vijaya Krishna T, Madhu Mohan T, Madhusudana Rao P. Thermodynamic and volumetric behavior of green solvent 1-butyl-3-methylimidazolium tetrafluoroborate with

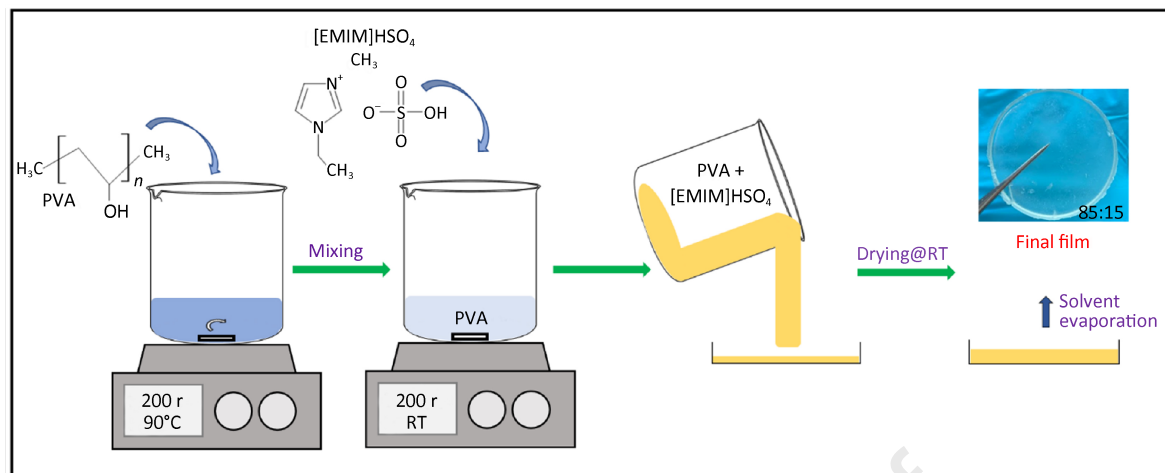
- aniline from $T=(293.15 \text{ to } 323.15)\text{K}$ at atmospheric pressure. *J Chem Thermodyn* 2016;100:165–76.
- [28] Jipa I, Stoica A, Stroescu M, Dobre L-M, Dobre T, Jinga S, et al. Potassium sorbate release from poly(vinyl alcohol)-bacterial cellulose films. *Chemical Papers* 2012;66.
- [29] Zhang Q-G, Wang N-N, Yu Z-W. The Hydrogen Bonding Interactions between the Ionic Liquid 1-Ethyl-3-Methylimidazolium Ethyl Sulfate and Water. *J Phys Chem B* 2010;114:4747–54.
- [30] Ricciardi R, Auriemma F, De Rosa C, Lauprêtre F. X-ray Diffraction Analysis of Poly(vinyl alcohol) Hydrogels, Obtained by Freezing and Thawing Techniques. *Macromolecules* 2004;37:1921–7.
- [31] Bunn CW. Crystal structure of polyvinyl alcohol. *Nature* 1948;161:929–30.
- [32] Structuring of Ionic Liquids. *Fundamentals of Ionic Liquids*, Wiley; 2017, p. 55–80.
- [33] Remiš T, Bělský P, Kovářík T, Kadlec J, Ghafouri Azar M, Medlín R, et al. Study on Structure, Thermal Behavior, and Viscoelastic Properties of Nanodiamond-Reinforced Poly (vinyl alcohol) Nanocomposites. *Polymers (Basel)* 2021;13:1426.
- [34] Park J-S, Park J-W, Ruckenstein E. Thermal and dynamic mechanical analysis of PVA/MC blend hydrogels. *Polymer (Guildf)* 2001;42:4271–80.
- [35] Gomaa MM, Hugenschmidt C, Dickmann M, Abdel-Hady EE, Mohamed HFM, Abdel-Hamed MO. Crosslinked PVA/SSA proton exchange membranes: correlation between physiochemical properties and free volume determined by positron annihilation spectroscopy. *Physical Chemistry Chemical Physics* 2018;20:28287–99.
- [36] Gengenbach TR, Major GH, Linford MR, Easton CD. Practical guides for x-ray photoelectron spectroscopy (XPS): Interpreting the carbon 1s spectrum. *Journal of Vacuum Science & Technology A: Vacuum, Surfaces, and Films* 2021;39.
- [37] Yang X, Guo Y, Liang S, Hou S, Chu T, Ma J, et al. Preparation of sulfur-doped carbon quantum dots from lignin as a sensor to detect Sudan I in an acidic environment. *J Mater Chem B* 2020;8:10788–96.
- [38] B J Lindberg, K Hamrin, G Johansson, U Gelius, A Fahlman, C Nordling, et al. Molecular Spectroscopy by Means of ESCA II. Sulfur compounds. Correlation of electron binding energy with structure. *Phys Scr* 1970;1:286–98.
- [39] Mohtasebi A, Chowdhury T, Hsu LHH, Biesinger MC, Kruse P. Interfacial Charge Transfer between Phenyl-Capped Aniline Tetramer Films and Iron Oxide Surfaces. *The Journal of Physical Chemistry C* 2016;120:29248–63.
- [40] Ningaraju S, Ravikumar HB. Studies on electrical conductivity of PVA/graphite oxide nanocomposites: a free volume approach. *Journal of Polymer Research* 2017;24:11.
- [41] Othman L, Chew KW, Osman Z. Impedance spectroscopy studies of poly (methyl methacrylate)-lithium salts polymer electrolyte systems. *Ionics (Kiel)* 2007;13:337–42.
- [42] Aziz SB, Woo TJ, Kadir MFZ, Ahmed HM. A conceptual review on polymer electrolytes and ion transport models. *Journal of Science: Advanced Materials and Devices* 2018;3:1–17.
- [43] Porcarelli L, Gerbaldi C, Bella F, Nair JR. Super Soft All-Ethylene Oxide Polymer Electrolyte for Safe All-Solid Lithium Batteries. *Sci Rep* 2016;6:19892.

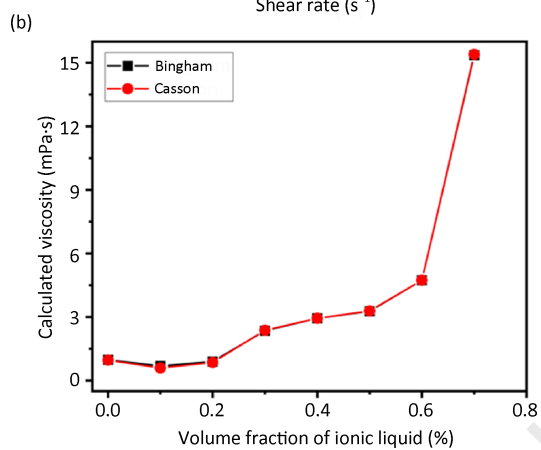
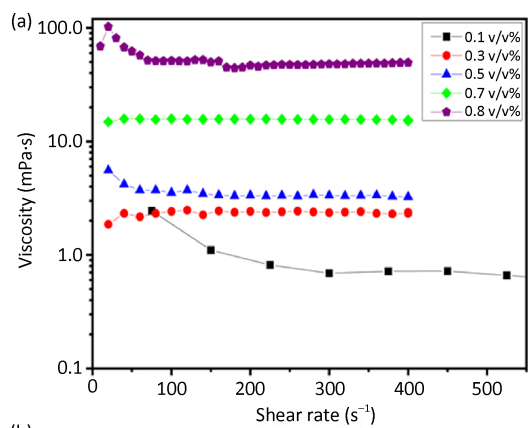
- [44] Tripathi M, Bobade SM, Kumar A. Nanocomposite polymer gel with dispersed alumina as an efficient electrolyte for application in supercapacitors. *Journal of Physics and Chemistry of Solids* 2021;152:109944.
- [45] Nakhanivej P, Rana HH, Kim H, Xia BY, Park HS. Transport and Durability of Energy Storage Materials Operating at High Temperatures. *ACS Nano* 2020;14:7696–703.
- [46] Tseng Y-H, Lin Y-H, Subramani R, Su Y-H, Lee Y-L, Jan J-S, et al. On-site-coagulation gel polymer electrolytes with a high dielectric constant for lithium-ion batteries. *J Power Sources* 2020;480:228802.
- [47] Sun Y, Liu B, Liu L, Yan X. Ions Transport in Electrochemical Energy Storage Devices at Low Temperatures. *Adv Funct Mater* 2022;32.
- [48] Karmakar A, Ghosh A. Dielectric permittivity and electric modulus of polyethylene oxide (PEO)–LiClO₄ composite electrolytes. *Current Applied Physics* 2012;12:539–43.
- [49] Kyritsis A, Pissis P, Grammatikakis J. Dielectric relaxation spectroscopy in poly(hydroxyethyl acrylates)/water hydrogels. *J Polym Sci B Polym Phys* 1995;33:1737–50.
- [50] Coşkun M, Polat Ö, Coşkun FM, Durmuş Z, Çağlar M, Türüt A. The electrical modulus and other dielectric properties by the impedance spectroscopy of LaCrO₃ and LaCr_{0.90}Ir_{0.10}O₃ perovskites. *RSC Adv* 2018;8:4634–48.
- [51] Abdulkadir BA, Dennis JO, Shukur MFBA, Nasef MME, Usman F. Study on Dielectric Properties of Gel Polymer Electrolyte Based on PVA-K₂CO₃ Composites. *Int J Electrochem Sci* 2021;16:150296.
- [52] Zhang S, Liu Z, Liu R, Du L, Zheng L, Liu Z, et al. A facile in-situ polymerization of cross-linked Poly(ethyl acrylate)-Based gel polymer electrolytes for rechargeable aluminum batteries. *J Power Sources* 2023;575:233110.
- [53] Chen W, Xing Z, Wei Y, Zhang X, Zhang Q. High thermal safety and conductivity gel polymer electrolyte composed of ionic liquid [EMIM][BF₄] and PVDF-HFP for EDLCs. *Polymer (Guildf)* 2023;268:125727.
- [54] Niu H, Ding M, Zhang N, Li X, Su X, Han X, et al. Preparation of imidazolium based polymerized ionic liquids gel polymer electrolytes for high-performance lithium batteries. *Mater Chem Phys* 2023;293:126971.
- [55] Hor AA, Yadav N, Hashmi SA. Enhanced energy density quasi-solid-state supercapacitor based on an ionic liquid incorporated aqueous gel polymer electrolyte with a redox-additive trimethyl sulfoxonium iodide. *J Energy Storage* 2023;64:107227.
- [56] Murphy JN, Mendes T, Kerton FM, MacFarlane DR. Biorenewable Calcite as an Inorganic Filler in Ionic Liquid Gel Polymer Electrolytes for Supercapacitors. *ACS Omega* 2023;8:21418–24.
- [57] Rao A, Bhat S, De S, Cyriac V, S AR. Study of [EMIM] [EtSO₄] ionic liquid-based gel polymer electrolyte mediated with hydroquinone redox additive for flexible supercapacitors. *J Energy Storage* 2023;68:107716.
- [58] Mazuki NF, Khairunnisa K, Saadiah MA, Kufian MZ, Samsudin AS. Ionic transport study of hybrid gel polymer electrolyte based on PMMA-PLA incorporated with ionic liquid. *Ionics (Kiel)* 2023;29:625–38.

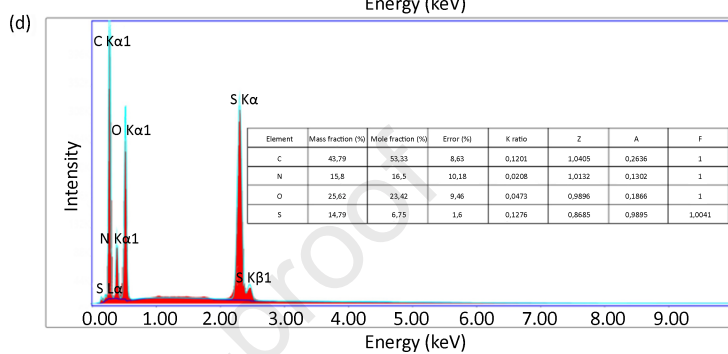
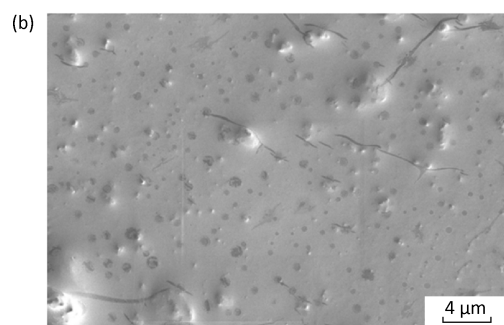
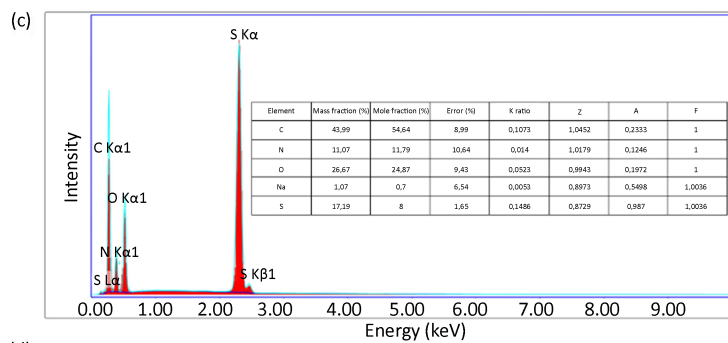
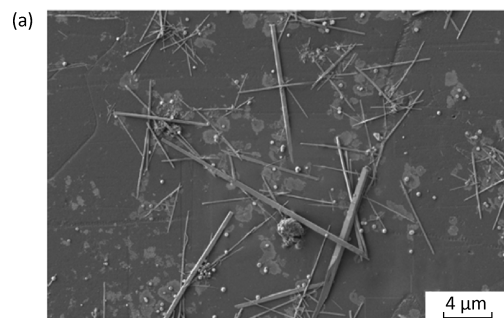
- [59] Singh A, Dhapola PS, Konwar S, Sharma T, Jun HK, Singh D, et al. Ionic liquid (1-ethyl-3-methyltricyanomethanide) doped polymer electrolyte (polyvinyl alcohol) for sustainable energy devices. *Journal of Science: Advanced Materials and Devices* 2023;8:100566.
- [60] Yao M, Ruan Q, Wang Y, Du L, Li Q, Xu L, et al. A Robust Dual-Polymer@Inorganic Networks Composite Polymer Electrolyte Toward Ultra-Long-Life and High-Voltage Li/Li-Rich Metal Battery. *Adv Funct Mater* 2023;33.

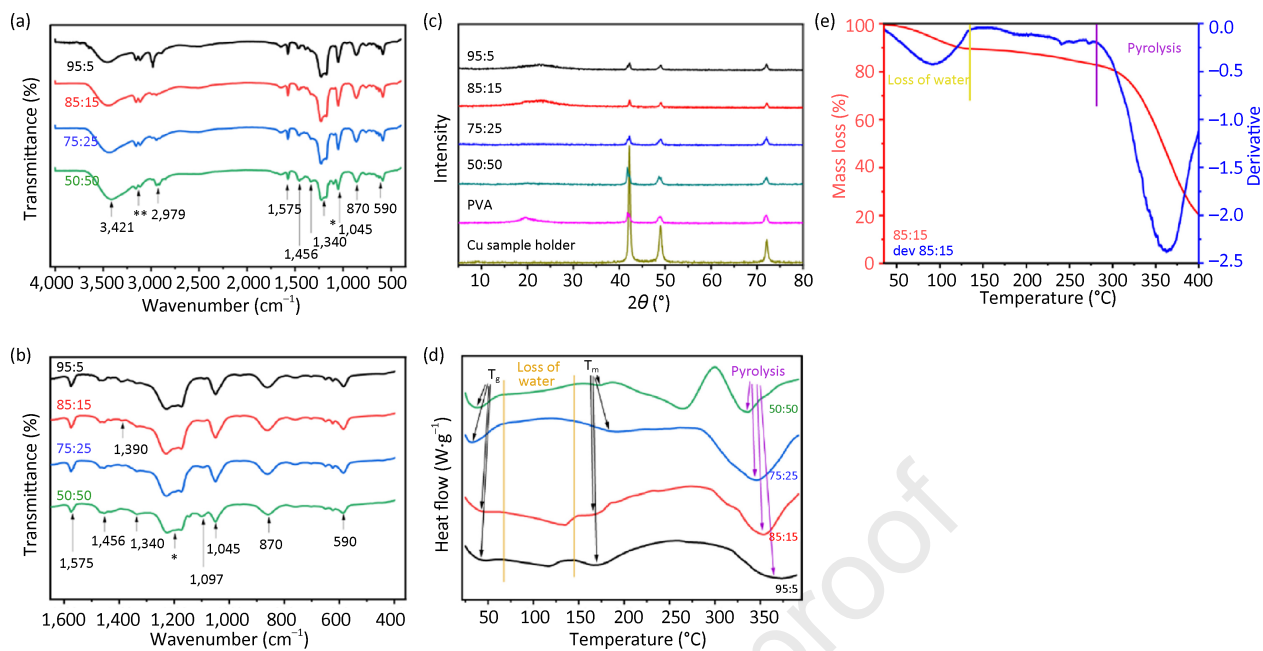
Journal Pre-proof

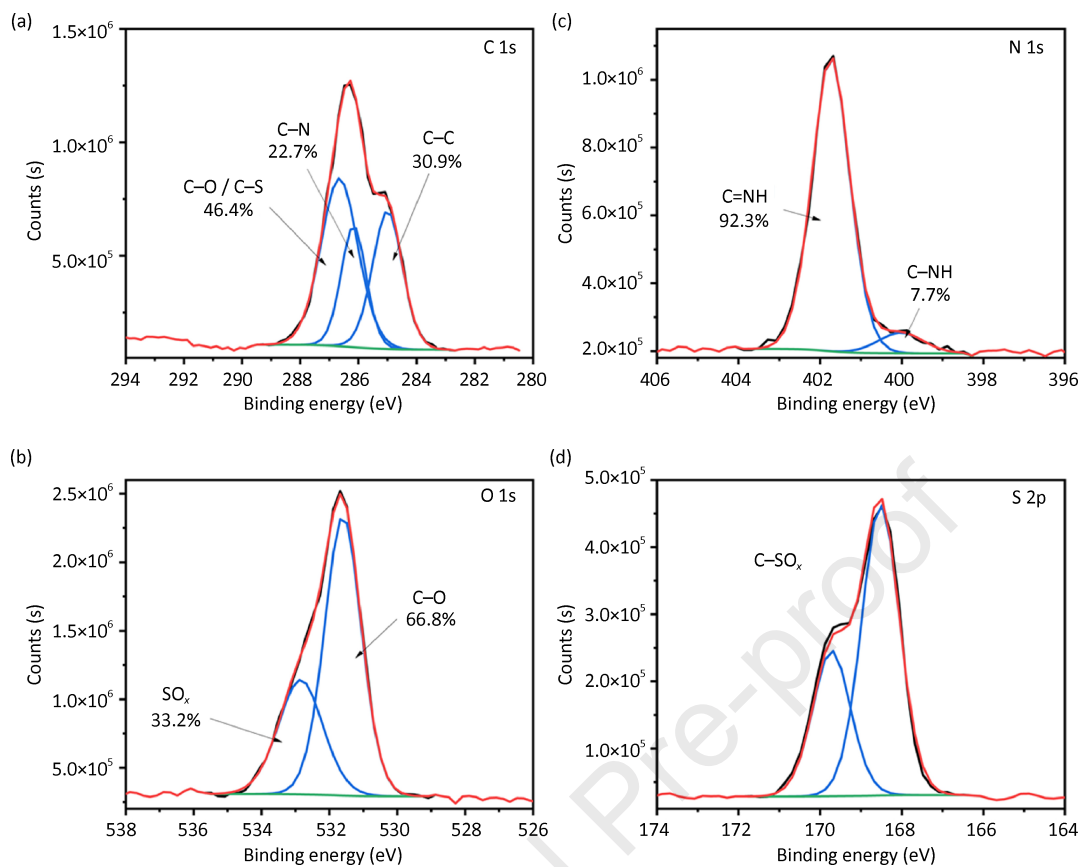


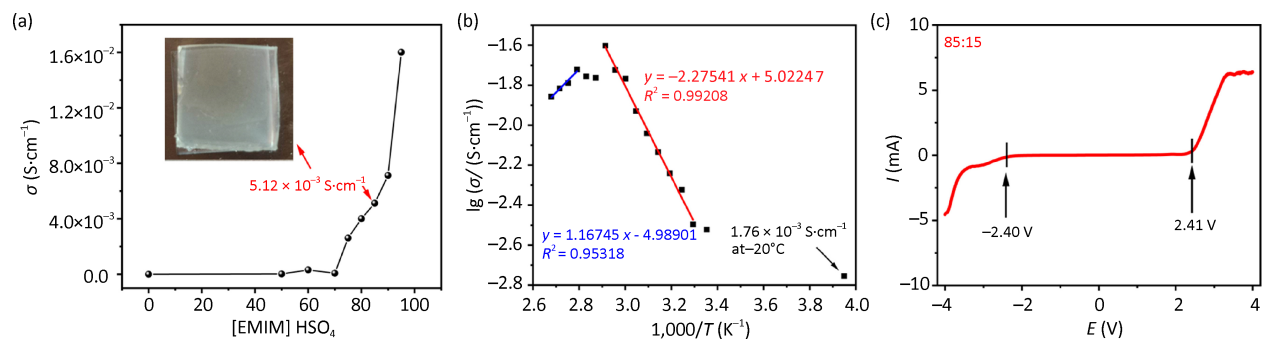


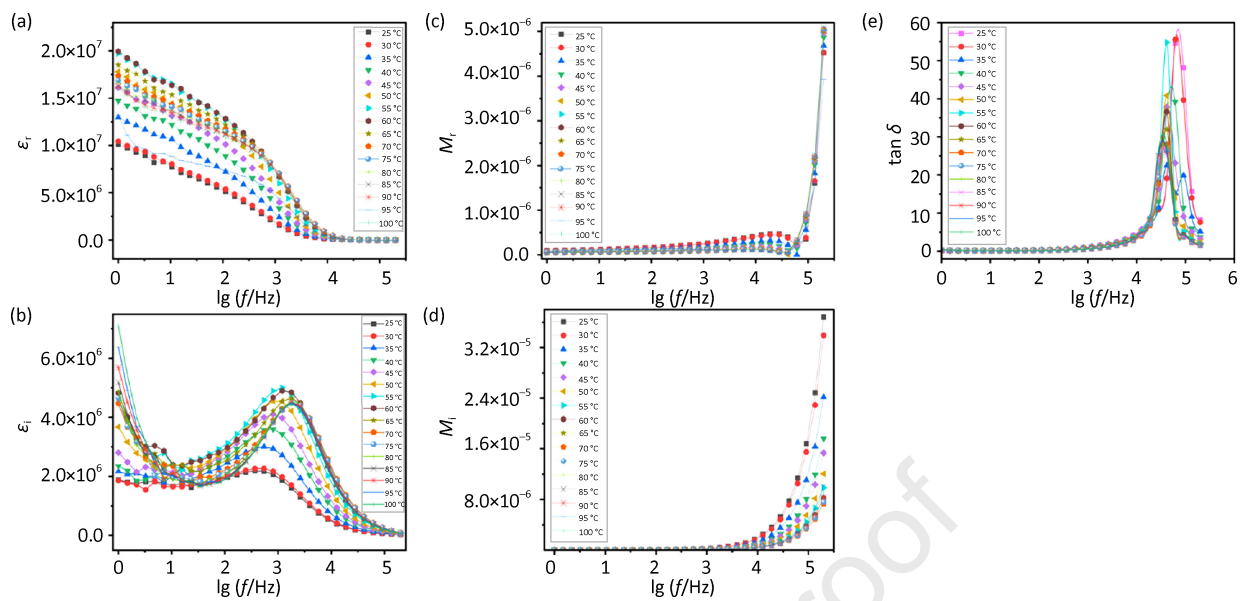


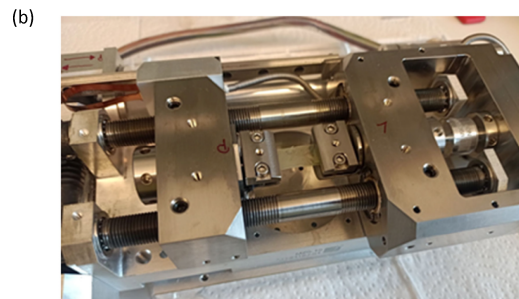
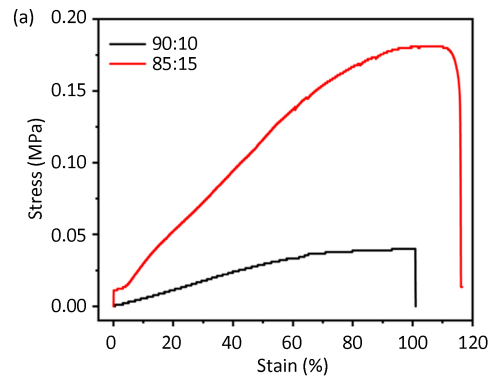


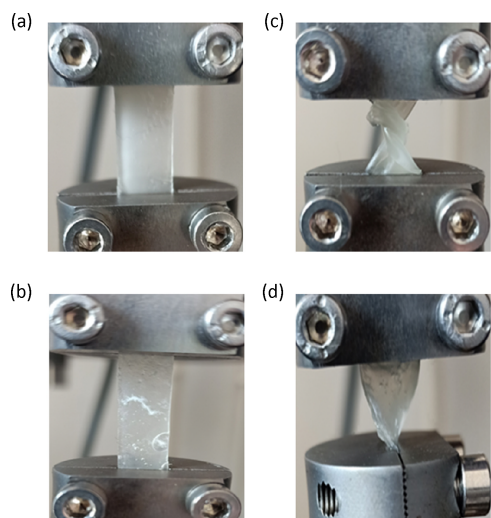




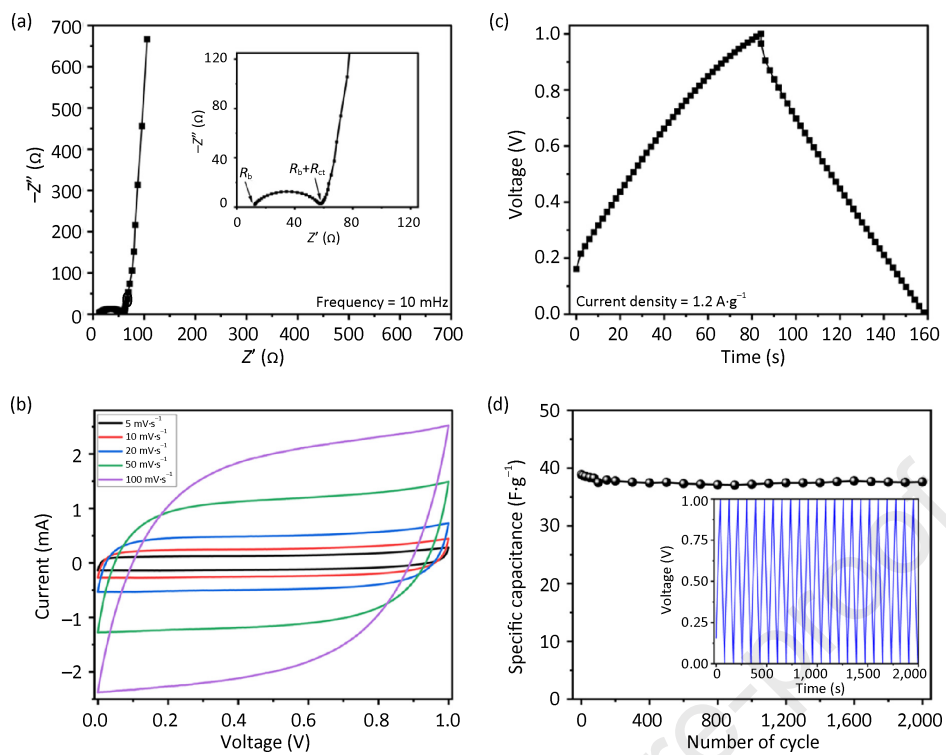








Journal Pre-proof



Highlights

- High performance and flexible ionogels (PVA:[EMIM]HSO₄) is designed for energy storage application.
- Ionogel exhibits room temperature ionic conductivity of $\sim 5.12 \times 10^{-3}$ S/cm with a wide potential window of ~ 4.81 V.
- Films shows excellent tensile and twisting properties even up to 360°.
- The films were tested for supercapacitor application with MWCNT electrodes.

Journal Pre-proof

Dr Amrita Jain (First and Corresponding author)

Amrita Jain received her Ph.D. from Jaypee University of Engineering and Technology, India, in 2014 in the field of energy storage devices, particularly supercapacitors. At present she is working as an Assistant Professor in the Department of Mechanics of Materials, Institute of Fundamental Technological Research, Polish Academy of Science, Warsaw, Poland. Her research area includes the development of sustainable materials for energy storage and dye adsorption application. She is also engaged in the development of gel polymer electrolytes for energy storage application.

Journal Pre-proof

Conflict of Interest

The authors declare that they have no known competing financial interests or personal relationships that could have appeared to influence the work reported in this paper.

Journal Pre-proof